Structural Analysis of DNA Bending Induced by Tethered Triple Helix Forming Oligonucleotides†

Taishin Akiyama and Michael E. Hogan*

Department of Molecular Physiology and Biophysics, Baylor College of Medicine, One Baylor Plaza, Houston, Texas 77030

Received September 26, 1996; Revised Manuscript Received December 20, 1996⊗

ABSTRACT: In order to monitor DNA flexibility, we have recently reported the design of an artificial DNA bending system consisting of two triple helix forming oligonucleotides (TFOs) connected by a flexible linker [Akiyama, T., & Hogan, M. E. (1996) *Proc. Natl. Acad. Sci. U.S.A.* 93, 12122−12127], which spans a single turn of DNA helix. Those data suggested that up to 60° of bending deformation could be induced with an expenditure of energy which is much smaller than predicted from bulk flexibility parameters. In this report, the detailed structure of the bend has been investigated by three different methods: circular permutation analysis, phasing analysis, and ring closure. Circular permutation and phasing analysis suggest that the magnitude of the bend is dependent on linker length. The apparent location of the bend was estimated from circular permutation analysis to be at the duplex region intervening the two sites of triple helix formation. The electrophoretic mobility of the bent complex appears to vary with the sequence of the intervening duplex region of the binding site complex, in the order of AT-rich > random ≥ GC-rich sequence. Detailed fitting of the phasing data has shown that bending is not accompanied by significant twisting deformation. Ring closure analysis with T_4 DNA ligase has confirmed the general magnitude of the TFO-induced bend and has additionally suggested that formation of the simple linear antiparallel triple helix does not enhance DNA flexibility.

The interaction between the biological compounds such as proteins and DNA is frequently accompanied with a global or local change of three-dimensional structure. These conformational changes may be crucial for molecular recognition and biological function. Numerous examples of protein-induced bends have been reported (Thompson & Landy, 1988; Kerppola & Curran, 1991a,b; Li et al., 1995; Schroth et al., 1991; Kostrewa et al., 1991; Pil et al., 1993; Wechstler & Dang, 1992; Fisher et al., 1992; Horikoshi et al., 1992; Shuey & Parker, 1986), and it has been suggested that protein-induced bends might be essential for eukaryotic as well as prokaryotic transcription (Martin & Espinosa, 1993; Rees et al., 1993), replication (Beese et al., 1993), and recombination systems (Goodman & Nash, 1989). For example, recent X-ray crystallographic analyses of TATA binding factor (TBP)−DNA complex revealed a 80° DNA bend induced by TBP (Kim, J. L., et al., 1993; Kim, Y., et al., 1993), and it was proposed that this relatively large bend might be of importance for the interaction between general transcription factors and RNA polymerase II. As another interesting example, it has been shown that integration of proviral human immunodeficiency virus I can be targeted to a protein-induced bend *in vitro* (Bor et al., 1995; Muller et al., 1994; Pruss et al., 1994). Besides protein-induced bends, small molecular weight compounds such as cc-1065 (Sun et al., 1993) or *cis*-platin (Rice et al., 1988; Huang et al., 1995) are known to induce bending of the duplex upon covalent bond formation with a base moiety at the binding site. The possibility of a relation between the induced bend and the biological activity of these compounds has been discussed (Hederson & Hurley, 1995).

Intermolecular triple helix formation has been proven to be useful for the recognition of duplex DNA. High sequence specificity and relatively high affinity have encouraged the use of triple helix motifs as artificial repressors (Postel et al., 1991; Cooney et al., 1988; Grigoriev et al., 1993; Maher et al., 1990) and as a DNA binding agent to direct sequence-specific DNA cleavage (Moser & Dervan, 1987; Perrouault et al., 1993) or site-directed mutagenesis (Havre et al., 1993). Recently, we and others have independently reported the design of an artificial DNA bending agent by exploiting the antiparallel triple helix motif (Akiyama & Hogan, 1996a) and parallel triple helix motif (Liberles & Dervan, 1996). In these studies, DNA bending was achieved by the binding of a tethered triple helix forming oligonucleotide (TFO),[1] which has a variable length of linker, connecting two oligonucleotide domains which form a triple helix at noncontiguous sites on the duplex (Figure 1). Phasing analysis in these studies (Akiyama & Hogan, 1996a; Liberles & Dervan, 1996) has suggested that the induced bending is directed toward the minor helix groove, as expected from simple modeling (Figure 1). In both studies, the bend angle was found to be dependent on the linker length in the tethered TFO. In our study, a geometrical calculation and a semi-empirical relation between the electrophoretic mobility and bending angle both suggested 50−70° as the largest bend angle in the series (Akiyama & Hogan, 1996a). Surprisingly, the difference in the binding affinity between the 50−70° bent triple helix and unbent triple helix was only a factor of 2−4, suggesting that the free energy required to induce a 50−70° bend is only 0.4−0.9 kcal/mol (Akiyama & Hogan, 1996a). That

† This work is supported by grants to M.E.H. from the Texas Advanced Technology Program and Aronex Pharmaceuticals, Inc.

* To whom correspondence should be addressed. Telephone: (713) 798−3892. FAX: (713) 798-6033. E-mail: mhogan@bcm.tmc.edu or takiyama@bcm.tmc.edu.

⊗ Abstract published in *Advance ACS Abstracts,* February 1, 1997.

[1] Abbreviations: TFO, triple helix forming oligonucleotide; SD, standard deviation.

S0006-2960(96)02429-4 CCC: $14.00

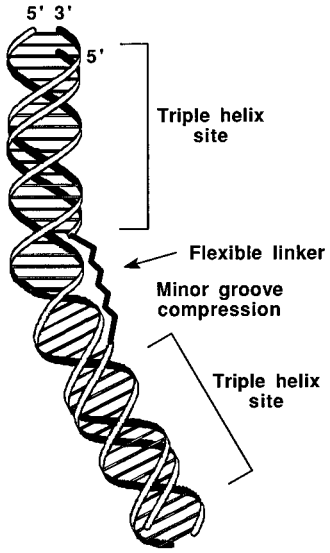

FIGURE 1: Schematic structure of an artificial DNA bend induced by tethered triple helix forming oligonucleotides. The cartoon depicts two 15 base long triple helix forming oligonucleotides (TFOs) bound to the major helix groove separated by a 10 bp duplex spacer. The polymer linker which connects oligonucleotide elements is depicted by a jagged solid line.

unexpectedly small bending free energy is *inconsistent* with that calculated from a simple elastic coil model (3.5 kcal/mol for 50° bending). Detailed thermodynamic and kinetic analyses via gel titration have led to a hypothesis that duplex flexibility is asymmetric, with compression of the minor helix groove of the DNA duplex being far easier than bending toward the major helix groove or bending toward the phosphate backbones (Akiyama & Hogan, 1996b). This hypothesis could be compromised if the observed high flexibility were somehow due to as yet unknown properties of triple helix structure. For example, the simple act of triple helix formation might give rise to bending or a local increment of DNA flexibility, thereby softening the duplex with respect to bending deformation. Additionally, the data at hand do not rule out a possibility that the observed bending might also be associated with unwinding or twisting deformation. To address such questions, we have investigated details of the structure and flexibility of the induced bend, via circular permutation analysis (Wu & Crothers, 1984), phasing analysis (Zinkel & Crothers, 1987), and ring closure analysis using T_4 DNA ligase (Shore et al., 1981).

MATERIALS AND METHODS

Chemicals and Enzymes. Restriction endonucleases, calf intestine alkaline phosphatase, and DNA polymerase I Klenow fragment were purchased from Boehringer Mannheim. T_4 DNA ligase and T_4 polynucleotide kinase were from Life Technologies. [γ-^{32}P]ATP was from Du Pont. Deoxynucleoside phosphoramidites were from Millipore. The linker phosphoramidites were from Glen Research.

Data Analysis. Curve fitting to the experimental data was executed with Deltagraph Pro3 on Macintosh IIci, in which a nonlinear least-squares analysis was used. Experimental errors are given as the standard deviation (SD). The number of repetitions (n) for each experiment were as follows: circular permutation analysis (Figure 3c and Table 1), $n = 3$; electrophoretic mobility versus linker length (Table 2), $n = 4$; phasing analysis (Figure 4c,d), $n = 5$.

Oligonucleotide Syntheses and Plasmid Construction. Oligonucleotides were synthesized using the solid phase phosphoramidite method on a Millipore Expedite Synthesizer, and were purified on a 18% (19:1 cross-linked) polyacrylamide gel (PAGE) containing 7 M urea as described (Akiyama & Hogan, 1996a,b). The construction of the bending vector (pBend4-NOBMIX) and the phasing vector (pSB-NOBMIX 10−20) was described previously (Akiyama & Hogan, 1996a).

Circular Permutation Analysis and Comparison of Gel Mobility of Triple Helices Formed by Various TFOs. Plasmid pBend4-NOBAT, NOBMIX, or NOBGC ($\approx 2 \times 10^{-7}$ M) containing the triple helix binding site (Figure 2b) was digested with a panel of restriction enzymes so as to alter the location of the bending site. After a standard phenol extraction and ethanol precipitation, plasmid DNA fragments were incubated with the TFOs (2×10^{-7}M) in 10 mM Tris-HCl (pH 7.5), 10 mM $MgCl_2$, and 10% sucrose at 37 °C for 16 h. Incubation mixtures were then loaded directly onto 8% nondenaturing PAGE (19:1, cross-linking). The gel was run in 89 mM Tris−borate and 10 mM $MgCl_2$ (TBM) buffer for 6 h (12.5 V/cm) and stained with 0.5 μg/mL ethidium bromide solution, followed by destaining with H_2O.

Phasing Analysis. The pSB-NOBMIX 10−20 plasmid set (Akiyama & Hogan, 1996a) was digested with *Pst*I and *Rsa*I. After a standard phenol extraction and ethanol precipitation, the digested products ($\approx 2 \times 10^{-7}$ M) were incubated with the TFOs (2×10^{-7} M) in 10 mM Tris-HCl (pH 7.5), 10 mM $MgCl_2$, and 10% sucrose at 37 °C for 16 h. The incubation mixtures were then analyzed by 6% nondenaturing PAGE (19:1). The gel was run in TBM buffer for 6 h (12.5 V/cm) and stained with 0.5 μg/mL ethidium bromide solution followed by destaining with H_2O or, as an alternative, stained with SYBR Green I (Molecular Probes).

Ring Closure Analysis. The *Xho*I restriction fragment (171 base pairs) of pBend4-NOBMIX was dephosphorylated by calf intestine alkaline phosphatase, and was end-labeled with [γ-^{32}P]ATP and T_4 polynucleotide kinase. The labeled DNA ($\approx 1 \times 10^{-9}$ M) was incubated with TFO (1×10^{-7} M) in 70 μL of 10mM Tris-HCl (pH 7.5) and 10 mM $MgCl_2$ at 37 °C for 5 h to form triple helix. The resulting triple helix solution was diluted to 90 μL, the final buffer condition being 50 mM Tris-HCl (pH 7.5), 5 mM KCl, 10 mM $MgCl_2$, 0.01% Nonident P-40, and 1 mM ATP. After equilibration for 10 min at 20 °C, 10 μL of T_4 DNA ligase was added to the solution to a final concentration of 100 units/mL. Aliquots (10 μL) were quenched as a function of time by adding to 1 μL of 0.5 M EDTA, and subsequent heating to 55 °C for 10 min. Samples were loaded onto 7% nondenaturing PAGE (19:1 cross-linked), and the gel was run in 89 mM Tris−borate and 10 mM EDTA (11 V/cm) for 3.5 h. Dried gels were visualized by autoradiography and were quantified with a Betascope 603 Blot analyzer (Betagen).

RESULTS

An antiparallel triple helix motif (Durland et al., 1991; Beal & Dervan, 1991) stabilized by G•GC and T•AT triplets was employed. In this triple helix structure, TFO lies within the major groove, and binding is stabilized by reverse Hoogsteen hydrogen bonding. Because protonation is not required to maintain triplet hydrogen bonding in this motif, binding is stable under neutral pH conditions (Durland et al., 1991; Beal & Dervan, 1991). Two unlinked TFOs (TAIL

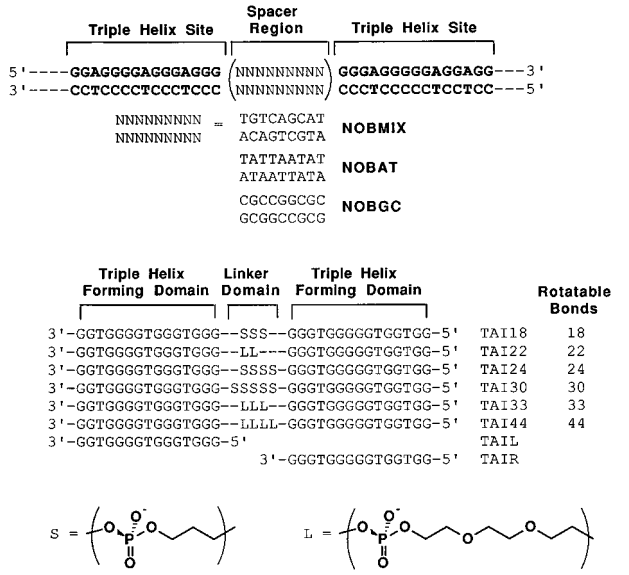

FIGURE 2: Sites for linked triple helix formation. Sites for triple helix formation site (top) are in boldface. The duplex sequence in parentheses is the one turn long intervening spacer region at which the bending is induced. The sequence of only the TFO binding site is shown. Subcloning of the binding site set into the pBend4 plasmid was described previously (Akiyama & Hogan, 1996a,b). Two domains of antiparallel triple helix forming oligonucleotide are connected by a flexible linker domain (bottom). S and L represent a propylene glycol phosphodiester unit and a triethylene glycol phosphodiester unit, respectively.

and TAIR) and six tethered TFOs were prepared, consisting of two triple helix forming regions connected by a linker. The linker moiety was created from either propylene glycol phosphodiester subunits (TAI18, -24, and -30) (Seela & Kaiser, 1987; Cload et al., 1993) or triethylene glycol phosphodiester subunits (TAI22, -33, and -44) (Durand et al., 1990) (Figure 2). Commercially available phosphoramidites corresponding to these linker phosphodiester units allow their incorporation within an oligomer using a standard DNA synthesizer. All TFOs were purified by denaturing polyacrylamide gel electrophoresis. Oligonucleotide purity (approximately $\geq$95%) was confirmed by polyacrylamide gel analysis of 5′-^{32}P-labeled oligomers (data not shown). Three unique binding sites were prepared. These binding site complexes have two noncontiguous sites of triple helix formation separated by approximately one helical turn of intervening duplex with either 100% GC (NOBGC), 50% GC (NOBMIX), or 0% GC content (NOBAT) (Figure 2).

Circular Permutation Analysis. Polyacrylamide gel electrophoresis is now well characterized as a tool to quantify DNA bending (Wu & Crothers, 1984; Koo et al., 1986). Bending analysis is based upon a reptation model, in which linear DNA migrates in a snake-like fashion during polyacrylamide gel electrophoresis (deGennes, 1971; Doi & Edward, 1978; Lerman & Frisch, 1982; Lumpkin & Zimm, 1982). It is well-known that the electrophoretic mobility of linear DNA is dependent on the molecular weight and the total charge of the DNA fragment. In addition to these two parameters, the mean square of the end-to-end distance of DNA fragment is also a determinant of the electrophoretic mobility according to the reptation model (Lerman & Fresch, 1982; Lumpkin & Zimm, 1982). Since the end-to-end distance of DNA duplex ranging from several base pairs to several hundred base pairs is remarkably influenced by the existence and the extent of bending, a bent DNA fragment is found to display significantly smaller electrophoretic mobility than a straight DNA with the same contour length.

The circular permutation method was originally developed by Wu et al. (Wu & Crothers, 1984), and then Levene et al. (Levene & Zimm, 1989), who quantified this method by using a new reptation model which included a contribution from elasticity. This method is based on the principle that the electrophoretic mobility of a DNA fragment with a bend depends on the distance from the end of the DNA fragment to the bend; thus, the electrophoretic mobility of a bent DNA is most retarded when the bend is located at the center (Wu & Crothers, 1984). We have prepared three sets of DNA fragments for circular permutation analysis. Each set differs in the sequence of the intervening duplex region of the binding complex (Figure 2). The DNA fragments in each set have identical length (171 base pairs) and almost the same base composition, but there is a difference in the location of the site for triple helix formation among the DNA fragments (Figure 3a). The invariant electrophoretic mobility of all DNA fragments in a polyacrylamide gel (data not shown) suggests that the sites of triple helix formation have no detectable intrinsic bend. When TAI18, which has the shortest linker in the series of the tethered TFOs, binds to the NOBMIX DNA fragment set (Figure 2), it is obvious that the electrophoretic mobility of the bound complex varies with the location of the binding site (Figure 3b; left). The *Eco*RV fragment possessing the binding site at the center shows the smallest electrophoretic mobility in the set of DNA fragments, and the *Bam*HI fragment possessing the binding site at the end shows the largest mobility. On the other hand, when TAI44, which has the longest linker in the series of tethered TFOs, binds to the same fragment set, no difference in the mobility is observed among the DNA fragments (Figure 3b; right). These experimental data support the idea that the binding of TAI18 induces a bend in the triple helix forming site, but that binding of TAI44 does not.

In order to determine the location of the bend induced by TAI18, we have normalized the relative mobility of each restriction fragment to that of the *Bam*HI fragment (where the bend is near the end). In Figure 3c, these normalized data are plotted against the distance from an end of the DNA fragment to the center of the bound site complex. Previously, it has been shown that fitting a cosine curve to such relative circular permutation data allows an accurate extrapolation of the apparent bending center (Kerppola & Curran, 1991b). The curve drawn in Figure 3c results from fitting a cosine curve to the experimental data, and the minimum value of the fitting curve indicates the bending center at 88 $\pm$ 2 bp (Table 1) from the end closest to the *Bam*HI site. The positions of the bends in the other DNA fragment sets possessing NOBAT or NOBGC were determined as well by applying a cosine equation to the data, and are also exhibited in Table 1. If the bends were positioned exactly at the center of the intervening segment of duplex, the bending center would have been at 86 bp. Thus, within an experimental accuracy of about $\pm$2 bp, the bending centers appear to be located at the center of the duplex region separating the two sites of triple helix formation.

By using phased poly(dA) tracts as a standard bending locus, Thompson et al. (Thompson & Landy, 1988) derived a empirical relationship between the bending angle (θ) and the relative mobility of a DNA fragment with a bend at its center (μ_m), normalized to the mobility when the bend is at the end (μ_e):

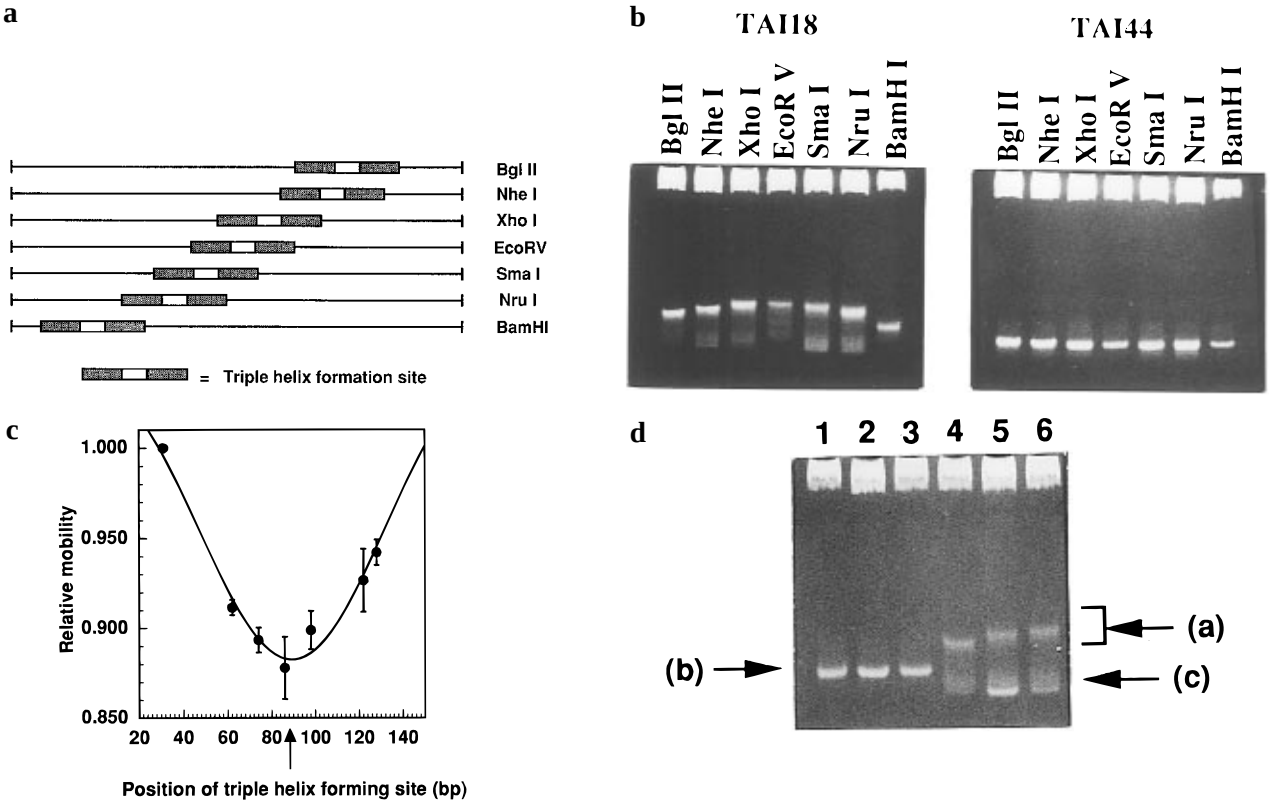

FIGURE 3: Circular permutation analysis. (a) DNA fragment set for the circular permutation analysis. The restriction DNA fragments generated from the pBend4 vector containing a triple helix binding site are illustrated as lines and boxes. Shaded boxes represent TFO binding sites, and a white box represents an intervening duplex region as described in Figure 2. Three sets of DNA fragments differing in the intervening region among 100% GC content (NOBGC), 50% GC content (NOBMIX), and 0% GC content (NOBAT) were prepared. (b) Circular permutation analysis. TAI18 (left) and TAI44 (right) complexes with the restriction fragment set (Figure 3a) were analyzed by 8% nondenaturing PAGE. The restriction fragments used are indicated on the top of the figure. For some restriction fragments (*Nhe*I, *Xho*I, *Sma*I, and *Nru*I), a small fraction of dissociated triple helix is detected as a second, uncomplexed band of free 171 bp duplex, but the dissociation effect observed here was not reproducible. (c) Determination of the bending center for the bound TAI18 complex. For each restriction fragment, the relative mobility of the bound TAI18 complex is presented relative to that of the *Bam*HI fragment. Data are plotted versus the distance from the helix end to the center of the binding site. Data are presented for the NOBMIX binding site, 50% AT content (Figure 2). The arrow indicates the apparent center of the bending as derived from curve fitting (see text). The curve represents the best fitting of a cosine curve to the data. Error bars refer to the SD of the mean of three different experiments. (d) The difference in the mobility of bent complexes among binding site complexes. Lanes 1, 2, and 3: TAI44-bound *Eco*RV fragments possessing NOBAT (0% GC content), NOBMIX (50% GC), and NOBGC (100% GC), respectively (Figure 2). Lanes 4, 5, and 6: TAI18-bound *Eco*RV fragments possessing NOBAT (0% GC), NOBMIX (50% GC), and NOBGC (100% GC), respectively (Figure 2). Arrow (a) and (b) indicate the TAI18-bound complex and TAI44-bound complex, respectively. Arrow (c) indicates the uncomplexed duplex.

Table 1: Apparent Center of the TFO-Induced Bend[a]

duplex	NOBAT	NOBMIX	NOBGC	theory
bending center (bp)	91 ± 7	88 ± 2	88 ± 5	86

[a] The location of the bend induced by TAI18 in each DNA fragment is represented as the base pair length from the end closest to the *Bam*HI site. Experimental error refers to a standard deviation of three different experiments. Theory refers to the separation between the end and the center of the site for linked triple helix formation.

$$\frac{\mu_m}{\mu_e} = \cos\frac{\theta}{2} \quad (1)$$

In the fragment set used in this study, μ_m and μ_e correspond to the electrophoretic mobility of the *Eco*RV fragment and that of the *Bam*HI fragment, respectively. The bending angle induced by each tethered TFO was calculated by applying the experimental data (μ_m/μ_e) to empirical eq 1 (Table 2). The largest bend in this series is achieved by the binding of TAI18 and is determined to be approximately 50−60° by this method. Interestingly, the binding of TAI30 and TAI33 appears to cause a small bend, even though the previous modeling study (Kessler et al., 1993) and a simple geometrical calculation (Akiyama & Hogan, 1996a; and the bottom row of Table 2) suggested that the binding of a tethered TFO with a linker greater than approximately 30 covalent bonds would not cause structural distortion in the intervening duplex. This second-order effect is discussed below.

Table 2: Bending Angle Induced by Tethered TFOs[a]

no. of linker bonds	**18**	**22**	**24**	**30**	**33**	**44**
NOBAT (deg)	47 ± 1	36 ± 6	35 ± 7	18 ± 5	14 ± 10	0 ± 0
NOBMIX (deg)	53 ± 7	48 ± 3	39 ± 6	27 ± 7	22 ± 6	0 ± 0
NOBGC (deg)	57 ± 4	47 ± 6	41 ± 5	30 ± 7	27 ± 12	0 ± 0
geometrical calcn (deg)	67	47	36	3	0	0

[a] For rows 1−3, bending angles were calculated according to the empirical eq 1 (Thompson & Landy, 1988). Experimental error refers to a standard deviation (SD) of at least four different experiments. For row 4, bending angles were calculated on the basis of a simple geometrical model (Akiyama & Hogan, 1996a).

It is noteworthy that the mobility of the bent DNAs induced by the same tethered TFOs varies with the sequence composition of the duplex region between the sites of triple helix formation in the order AT-rich > random ≥ GC-rich sequence (Figure 3d). This difference is inherent to the bent

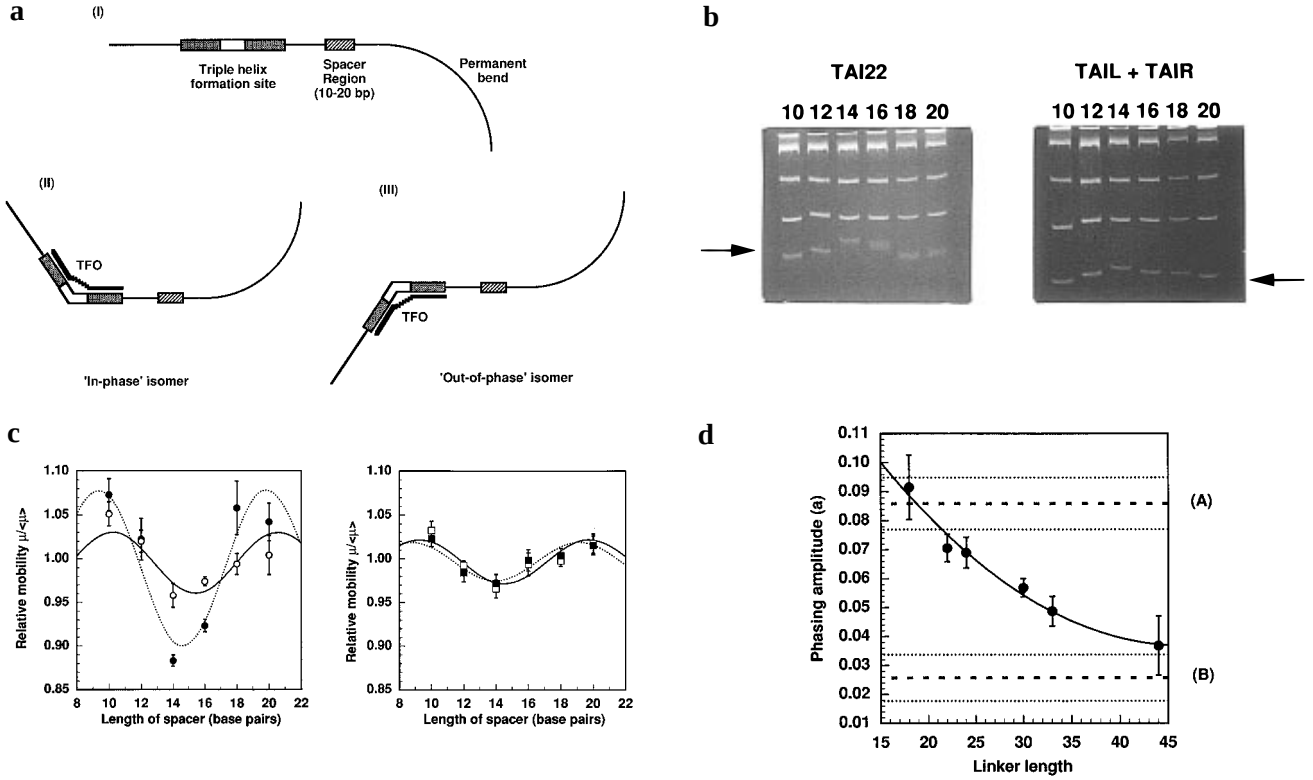

FIGURE 4: TFO-induced bending analysis via phase-sensitive vectors. (a) Structure of the DNA fragment used for phasing analysis. The cartoon illustrates the structure of the DNA fragment used for phasing analysis. A variable spacer region from 10 to 20 bp is placed between the triple helix formation site (Figure 2) and a permanent bend resulting from six consecutive phased AT tracts. The shape of the unbent complex (I) is practically independent of the spacer length (10−20 bp). Once a TFO with a short linker binds to the phasing fragment set, the bend induces a change of DNA shape which is a function of spacer length. The "in-phase" isomer (II) and "out-of-phase" isomer (III) are presented as the two extreme conformers. All other spacer lengths result in isomers with a shape in between those two limits. (b) Phasing analysis. The left panel is a PAGE analysis for the phase-sensitive set bound to TAI22. The right panel is a similar analysis for the complex formed with unlinked TAIR and TAIL oligomers. The numbers on the top of the panels display the number of base pairs in the spacer region. The bottom band of each lane (arrow) is the DNA fragment of interest, in the context of other fragments generated from the plasmid digest. (c) Plot of relative mobility versus spacer length. The electrophoretic mobility of phasing DNA fragments is plotted against the spacer length. Data have been normalized to the average mobility over the entire spacer range. Left panel: open circles (solid line), phasing behavior of TAI44-bound fragments; closed circles (dotted line), phasing behavior of TAI18-bound complex. Right panel: open squares (solid line), phasing behavior of the unlinked TAIL and TAIR complex; closed squares (dotted line), phasing behavior of free duplex. The lines are the best-fitting curves of the data to eq 3. (d) Phasing amplitude versus linker length. The phasing amplitude (*a*) derived from the fits as in Figure 4c is plotted against the number of covalent bonds in the linker region of the tethered TFOs. Broken line (A) is the phasing amplitude measured under identical gel conditions for the standard bending set, which displays a 54° bending angle, obtained with three phased oligo(dA) tracts (Levene et al., 1986; Thompson & Landy, 1988). Broken line (B) is the amplitude measured for the unlinked TAIL plus TAIR complex. Dotted lines parallel to the broken lines (A) and (B) show one standard deviation for amplitudes (*a*) derived for the oligo(dA) and unlinked TAIL plus TAIR standards. The curve connecting the data points is an empirical polynomial fit to the data.

complex, because the electrophoretic mobility of DNA fragments with no TFO (data not shown) or with TAI44 (Figure 3b) is independent of the sequence of the intervening duplex.

Phasing Analysis. Phasing analysis, which is one of the most sensitive methods to detect DNA bending, was carried out by using a phasing plasmid set (pSB10−20) originally described by Zinkel et al. (Zinkel & Crothers, 1987; Drak & Crothers, 1991). DNA fragments generated from the phasing plasmid set consist of a permanent, standardized curve resulting from a phased poly(dA) tract, plus a site for triple helix formation (NOBMIX), and a variable spacer region (Figure 4a). The spacer region is positioned between the permanent curve and the binding site complex, and can be varied from 10 to 20 bp by increments of 2 bp, thereby generating a set of six fragments. According to the reptation model, the electrophoretic mobility should be a function of the mean square of the end-to-end distance of DNA fragment. Since the uncomplexed triple helix binding site has no intrinsic bend, the end-to-end distance of the pSBNOBMIX 10−20 set will be altered minimally by variation of spacer length. However, if a bend is induced at the binding site complex, the overall shape of the DNA fragment will be dramatically affected by spacer length, influencing the end-to-end distance, in the range of conformational isomers between the "in-phase" and "out-of-phase" orientation of the permanent and induced bend (Figure 4a). Consequently, the electrophoretic mobility of this doubly bent DNA fragment should become a function of the spacer length. Figure 4b shows typical phasing experiments. When bound to the pSBNOBMIX 10−20 set, TAI22 (22 bond linker) induces a significant amplitude of phasing variation (the arrow in Figure 4b, left). The binding of the unlinked TFO pair (TAIL + TAIR) appears to induce a small amplitude of phase variation in the phasing fragment sets (Figure 4b, right). This subtle bending could not be detected by circular permutation analysis.

In the case of a linear DNA fragment possessing two independent bends, the end-to-end distance varies with the number of helical turns (*H*) of the region separating the center of the two linked bends. Consequently, the electrophoretic mobility of a bent fragment relative to the average mobility

Table 3: Phase Variation of Bent Complexes as a Function of Linear Span[a]

TFO	TAI18	TAI22	TAI24	TAI30	TAI33	av
n	0.010 ± 0.052	−0.050 ± 0.058	−0.026 ± 0.076	−0.046 ± 0.095	0.024 ± 0.074	−0.019 ± 0.078

[a] The parameter *n*, which represents the phasing variation of the bent complex, was calculated from the best fitting of the phasing data to eq 3. The theoretical range of *n* is from −1 to +1. The zero of the *n* requires that the induced bend compresses the minor helix groove. On the other hand, a value of −1 or +1 for *n* means that the induced bend serves to compress the major helix groove (see text). Experimental errors refer to 1 SD (standard deviation) of the mean of at least four different measurements.

of all fragments ($\mu/\langle\mu\rangle$) in phasing analysis can be expressed (Akiyama & Hogan, 1996a):

$$\frac{\mu}{\langle\mu\rangle} = a\cos\left[2\pi\left(H + \frac{n}{2}\right)\right] + d \text{ (provided that } a \geq 0 \text{ and } -1 \leq n < 1) \quad (2)$$

where *a* is the constant which depends on the magnitude of the bend and *d* is an offset term which depends on the conditions of electrophoresis. The constant *n* is determined by the directionality of the two bends. If two bends have the same directionality, the constant *n* should be close to the value of |1| in phasing analysis. Conversely, when the bends have opposite directionality, *n* should be zero. For the set of DNA fragments we used, the parameter *H* can be expressed as

$$H = \frac{x}{b_1} + \frac{B_1}{b_1} + \frac{B_2}{b_2} + \frac{B_3}{b_3}$$

where *x* is the length (bp) of the spacer region in the phasing fragments, and B_3, B_2, and B_1 are the lengths of half of an AT tract (30 bp), half of a triple helix site (15 bp), and the remainder of the plasmid (30 bp), respectively. The constants b_3, b_2, and b_1 are the helical pitch of the AT tract (10.34 bp/turn) (Drak & Crothers, 1991), that of the triple helix site (11.2 bp/turn) determined recently by Shin et al. (Shin & Koo, 1996), and that of the remainder of plasmid (10.49 bp/turn) (Drak & Crothers, 1991), respectively. Thus, eq 2 can be converted to

$$\frac{\mu}{\langle\mu\rangle} = a\cos\left[2\pi\left(\frac{x}{10.49} + 7.10 + \frac{n}{2}\right)\right] + d \quad (3)$$

Fitting the phasing data to eq 3 allows determination of the parameters *a*, *d*, and *n*. The parameter *n*, which provides information on the directionality of the bend, has been tabulated in Table 3. The value of *n* for each bend is almost constant and close to zero for each of the TFOs. Since a previous phasing study by Zinkel et al. (Zinkel & Crothers, 1987) has shown that the overall permanent bend resulting from six phased A tracts is directed toward the major helix groove at the apparent center of the bend, the data of Table 3 suggest that (1) all of the bends induced by the set of TFOs are directed toward the minor groove and (2) changing the length of the linker does not cause significant winding or unwinding deformation, since this would have induced a nonzero value of *n*.

The constant *a* in eq 3 is equivalent to the phasing amplitude (*a*) of the cosine curve fitted to the experimental data. This constant is related to the difference in mobility between the "out-of-phase" isomer and "in-phase" isomer (Figure 4a), and is therefore one way to quantify the magnitude of the induced bend. In Figure 4d, the experimentally determined value for *a* is plotted against the number of covalent bonds per linker in tethered TFOs. The data confirm that the extent of the bending is dependent on the length of the linker. This finding is entirely consistent with the results obtained from the circular permutation analysis (Figure 4a). Unfortunately, formulation of the relation between the phasing variation (*a*), the bending angle (θ), and the number of covalent single bonds in the linker is not a simple matter. However, we are able to estimate the induced bend angle very roughly by comparing the phasing amplitude (*a*) induced by the binding of tethered TFOs with that of a standard bend, which possesses a permanent bend composed of three phased poly(dA) tracts instead of the triple helix formation region. Analysis of the standard phasing set (data not shown) gave a phasing amplitude (*a*) of 0.0859 ± 0.0081, illustrated as the broken line (A) in Figure 4d. Previous work (Levene et al., 1986; Thompson & Landy, 1988) has shown that this standard bend should be approximately 54°. Thus, relative to that standard, value *a* resulting from the binding of TAI18 (0.0915 ± 0.0096) appears to correspond to an approximately 60° bend, which is very close to the bend angle estimated by the circular permutation analysis and simple geometrical considerations [Table 2 and Akiyama and Hogan (1996a)].

When TAI44 (44 bond linker) binds to the fragment set, the phasing amplitude *a* was found to be 0.0368 ± 0.0089, which is very close to the amplitude (0.0256 ± 0.0069) obtained upon binding the unlinked TFO pair [broken line (B), Figure 4d]. Relative to experimental error, we conclude that TAI44 does not cause a significant bend as compared to the unlinked TFOs (TAIL and TAIR).

Ring Closure Analysis. The reaction of DNA ligase with a linear DNA with 5′-phosphorylated cohesive ends can proceed through either intermolecular or intramolecular ligation (Figure 5a). The ratio of the intramolecular cyclization reaction rate constant k_1 to that of the bimolecular reaction k_2, referred to as the *J*-factor, is a measure of ring closure efficiency (Shore et al., 1981; Taylor & Hagerman, 1990; Kahn & Crothers, 1992; Levene & Crothers, 1986a,b; Shore & Baldwin, 1983; Koo et al., 1990). The *J*-factor is a function of the contour length and the number of helical DNA turns, which define the effective concentration of one end of a helix in the region nearby the other, the angular correlation between the two ends, and the torsional angle between the two ends. Monte-Carlo simulation predicts (Levene & Crothers, 1986a) and experiments have established (Kahn & Crothers, 1992; Koo et al., 1990) that a bend in the helix axis of DNA influences the effective concentration and the angular correlation of the two ends so as to increase the *J*-factor significantly.

The 171 bp *Xho*I fragment of the circular permutation vector was employed as a substrate for the ring closure analysis. Ring closure efficiency for a DNA fragment of this length should be very sensitive to the existence of a bend (Koo et al., 1990). Typical examples of ring closure reaction kinetics are shown in Figure 5b, and the reaction profiles are summarized in Figure 5c. The intramolecular reaction

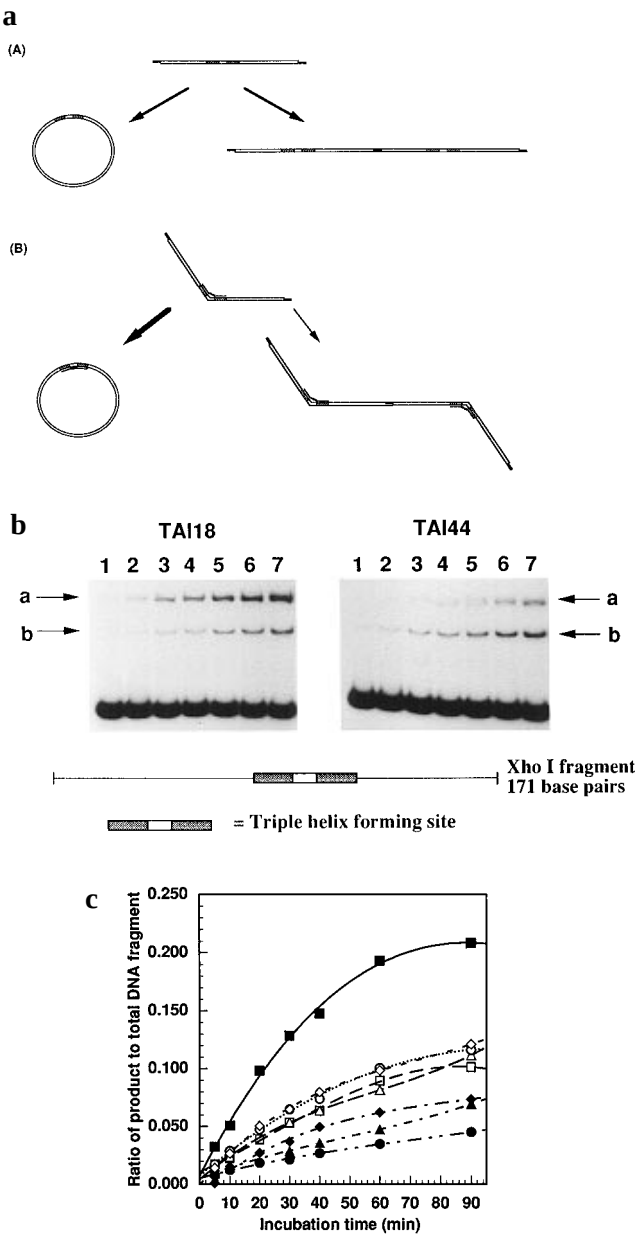

FIGURE 5: Bending analysis via ring closure analysis (a) Principle of the ring closure analysis. (A) Reaction of an unbent DNA catalyzed by T_4 DNA ligase. The first step in the ligation reaction of a DNA fragment possessing two complementary ends can generate both a circular monomer and a linear dimer as products. (B) When there is a bend in the DNA substrate, the intramolecular circularization reaction is stimulated as compared to the reaction of straight DNA as a substrate. (b) Ring closure kinetics. Ring closure kinetics were investigated for the TAI18 (left) and TAI44 (right) complexes with the *Xho*I fragment of pBend4 bearing the NOBMIX binding site (Figure 2). The reaction mixtures, catalyzed by T_4 DNA ligase, were analyzed by native PAGE. Arrow a indicates the circular monomer product from the T_4 DNA ligase reaction. Arrow b indicates the linear dimer. The incubation time with T_4 DNA ligase at 20 °C is as follows: lane 1, the incubation mixture was quenched immediately after the addition of T_4 DNA ligase; lane 2, 5 min; lane 3, 10 min; lane 4, 20 min; lane 5, 30 min; lane 6, 40 min; lane 7, 60 min; lane 7, 90 min. (c) Ratio of ligation products to the total substrate DNA. The ratio of each product is plotted against the reaction time by T_4 DNA ligase. In all cases, closed symbols refer to kinetics for the circular monomer, while open symbols refer to kinetics for formation of the linear dimer. Square symbols refer to the reaction kinetics for the TAI18-bound complex, circles refer to the unlinked TAIL,R complex, triangles refer to the TAI44-bound complex, and diamonds refer to unbound DNA. The curve connecting the data points is an empirical polynomial fit to the data. Data are the average of two independent experiments.

to produce a circular monomer (closed symbols) is significantly accelerated by the binding of TAI18, as compared to that resulting from the binding of TAI44 or the unlinked pair of TFOs (Figure 5c). On the other hand, none of the TFOs produce a significant change in the rate of linear dimer formation (open symbols). Since the other parameters affecting J should be considered as almost identical, the stimulation of the cyclization reaction by the binding of TAI18 is easily ascribed to bending. It should be noted that the binding of the unlinked TAIL and TAIR pair *suppresses* the ring closure rate (Figure 5c) as compared to the unbound complex, yet has no measurable effect on intermolecular dimer formation. Several theoretical (Levene & Crothers, 1986a,b) and experimental methods for quantitation of ring closure have been documented (Taylor & Hagerman, 1990; Kahn & Crothers, 1992; Shore & Baldwin, 1983). Our data are qualitatively consistent with these theories. A quantitative treatment of our data in the context of previous theory is in progress.

DISCUSSION

Since the triple helix motif is relatively simple and rigid as compared to the binding motif for DNA binding protein, it is reasonable to conclude that the difference in the binding free energy among bent triple helices provides a direct measurement of the deformational free energy resulting from induction of a bend (Akiyama & Hogan, 1996a,b). In this study, circular permutation analysis, phasing analysis, and ring closure analysis have all suggested that the binding of a series of tethered TFOs can induce bending which varies systematically with linker length. From detailed consideration of phasing analysis, we have concluded that systematic shortening of the linker length from 44 to 18 covalent bonds induces no appreciable twisting deformation of the DNA duplex. This result is consistent with modeling prediction (Akiyama & Hogan, 1996a) and is very important for the application of this bending system to quantify DNA flexibility. Based upon that analysis, we conclude that the deformational energy estimated from the comparison between the bent TAI18 complex and the unbent TAI44 complex appears to result only from the free energy of bending deformation.

A previous modeling study (Kessler et al., 1993) suggested that a linker comprising 25 covalent bonds might be adequate for spanning 2 triple helices separated by 1 helical turn of DNA duplex. In addition, our previous analysis using a static geometrical model also indicated that TAI33 and TAI44 would induce no bend (Akiyama & Hogan, 1996a; see the bottom row in Table 2). However, the data of this study (Figure 3a, Figure 4d, and Table 2) suggests that TAI30 or TAI33 appears to induce a small bend. From a simple geometrical viewpoint (Akiyama & Hogan, 1996a), if TAI33, for which the linker consists of 33 covalent bonds, causes a bend in 1 helical turn of duplex (33.5 Å), the average bond increment in the linker must be <1.02 Å. Assuming that the linker extends fully, which is a possible stable conformation of the linker, the average bond increment for such aliphatic linkers should be 1.1−1.2 Å (Dewar & Thiel, 1977), which is 10−20% longer than what the TAI33 data seem to specify (1.02 Å). We propose two possible explanations for this inconsistency. One explanation is that the apparent bend which we have detected is due to the induction of directional flexibility. Simple modeling suggests that, in the complexes we have formed, the linker runs parallel with the axis of the

duplex (Figure 1; right). This linker bridge could suppress the motion of the intervening duplex region so as to restrict flexural motions, which would have ordinarily lead to major groove compression. Zhurkin et al. (Zhurkin et al., 1991; Olson et al., 1993) have proposed that the sequence-dependent asymmetry in the thermal fluctuation of DNA can introduce the sequence-directed bends. That proposal is consistent with the above idea that increased stiffness with respect to major groove compression has induced a time-averaged minor groove bend for linkers as long as 30−40 bonds. Another explanation is that the assumption of full linker extension might be incorrect. Thus, our simple geometrical model is based on the idea that the covalent bonds connecting two triple helix domains might be all "anti". However, it is known that for the case of small organic compounds, the "gauche" conformer could be preferred to the "anti" conformer (Carey & Sundberg, 1984). Even though the results derived from such small molecules may not be exactly applicable to the structure of the linker that we have used in this study, which is a more complicated structure, it is possible that some of the covalent bonds might adopt the "gauche" conformer, which would result in shortening of the end-to-end distance of the linker moiety.

During our analysis of DNA bending, it was observed that the electrophoretic mobility of the bent DNA induced by the same TFO depended on the sequence of the duplex region between the two sites of triple helix formation (Figure 3d), which is consistent with previous results (Akiyama & Hogan, 1996a). Specifically, upon binding TAI18, the *Eco*RV restriction fragment of NOBAT (AT-rich intervening duplex) shows considerably faster mobility than those of NOBMIX (random) and NOBGC (GC-rich). The simplest interpretation of this finding is that the induced bending angle in the NOBAT complex is smaller than that in NOBMIX or NOBGC (Table 2). The mobility of these three DNA fragments is identical in the absence of TFO binding, which rules out the possibility of an intrinsic bending. With regard to the geometrical model of bent DNA (Figure 1), the bending angle is determined by the length of the intervening duplex and the length of the linker. In this case, because the bound TFO is identical, the simple geometric model suggests that the length of the intervening duplex must vary with sequence in these binding site, with the AT-rich duplex being shorter than the others. To the best of our knowledge, there is no clear dependency of base pair rise on the sequence in B-DNA structure. Thus, our data suggest a small difference in helical pitch as a function of GC content. However, the data are preliminary and do not warrant a more detailed analysis at present.

Phasing analysis, which is the most sensitive method we have used to detect bending, has shown that the binding of the unlinked TFO pair (TAIL and TAIR) induces small but measurable bending of the duplex (Figure 4). The magnitude of the bend induced by the binding of TAIL and TAIR could not be determined by circular permutation analysis of the unlinked complex. However, it must be significantly smaller than 10°, which would have been detectable by that assay. The origin of this $\ll 10°$ bend remains to be determined.

In the ring closure analysis carried out by us, the circularization rate of the DNA complex with TAI44 or the two unlinked TFOs (TAIL and TAIR) is equal to or slightly slower than that of the fragment without TFO (Figure 5c). As described above, the number of net helical turns in a duplex is critical for the determination of closure rate. The length of the DNA fragments in our studies is 171 bp, which is equal to 16.3 turns of helix, assuming 10.49 bp/turn (Drak & Crothers, 1991) for the helical pitch of B-DNA under the conditions used for ring closure analysis. Upon formation of two 15 bp segments of triple helix at 11.2 bp/turn (Shin & Koo, 1996), the helical twist for the 171 bp complex formed with two unlinked TFOs is calculated to be 16.1 ± 0.1 turn. Therefore, the binding of the unlinked TFOs (TAIL and TAIR) should have *increased* the closure rate and *J*-factor based solely on twist change. The fact that triple helix formation *decreased* the rate of the ring closure reaction (Figure 5c) suggests two important conclusions: (1) The remarkably high flexibility for minor groove compression, which we have detected (Akiyama & Hogan, 1996a,b), cannot be ascribed to the creation of a flexible hinge at or around the triple helix, since such a site would be easily detected by ring closure analysis, which is at present the most sensitive method to detect local sites of DNA flexibility (Kahn et al., 1994). (2) Antiparallel triple helix formation actually stiffens the duplex at or around the site of triple helix formation. Previously, Maher et al. proposed that parallel triple helix formation seemed to stiffen DNA (Maher et al., 1990). Our data are consistent with that proposal.

Previously, we have hypothesized that the deformational energy associated with minor helix groove compression is unusually small (Akiyama & Hogan, 1996a,b). The data described here have suggested that the observed high flexibility cannot be explained by the inherent structure or flexibility of the antiparallel triple helix. In addition, phasing analysis has shown that, as predicted from simple geometrical modeling (Akiyama & Hogan, 1996a,b), the small deformation energy observed by us is dominated by the contribution from bending energy, but not from twisting deformation. The tethered TFO-induced bending system developed in this study can introduce a bend in a relatively small segment of DNA duplex. The stable binding of TAI18 possessing 18 covalent bonds in the linker was shown to induce approximately 50−70° of bending, which is the largest in the series. We have also shown that by varying the length and structure of the linker phosphodiester unit, bends with various angles can be induced, as needed, in the duplex. Work is in progress to determine the maximum bending deformation which can be induced in DNA by this method and its energy cost. Functional replacement experiments, in which protein-induced bends are replaced with an intrinsic bend resulting from the phased A tracts, have revealed the importance of bends on RNA transcription (Kim et al., 1995; Bracco et al., 1989) and DNA recombination (Goodman & Nash, 1989). The triplex-induced bend described here is remarkably stable under physiological pH. This character may allow exploitation of this artificial bending system as a reagent to elucidate the importance of DNA bending in biological systems, and to modulate bending for the purpose of pharmaceutical or biotechnological purposes.

ACKNOWLEDGMENT

We thank Prof. D. Crothers (Yale University) for kindly providing phasing plasmids, Prof. D. P. Hollywood (Trinity University, Ireland) for technical advice, Mr. R. Tinder for oligonucleotide syntheses, and Dr. R. Mitra for useful discussion. We also thank Ms. Bonnie Iverson and Ms. Du Xiao for reading of the manuscript.

REFERENCES

Akiyama, T., & Hogan, M. E. (1996a) *Proc. Natl. Acad. Sci. U.S.A. 93*, 12122−12127.

Akiyama, T., & Hogan, M. E. (1996b) *J. Biol. Chem. 271*, 29126−29135.

Beal, P. A., & Dervan, P. B. (1991) *Science 251*, 1360−1363.

Beese, L. S., Debryshire, V., & Steitz, T. A. (1993) *Science*, *260*, 352−355.

Bor, Y.-C., Bushman, F. D., & Orgel, L. E. (1995) *Proc. Natl. Acad. Sci. U.S.A. 92*, 10334−10338.

Bracco, L., Kotlarz, D., Kolb, A., Diekman, S., & Buc, H. (1989) *EMBO J. 8*, 4289−4296.

Carey, F. A., & Sundberg, R. J. (1984) in *Advanced Organic Chemistry*, pp 93−160, Plenum Press, New York and London.

Chrambach, A., & Rodbard, D. (1971) *Science 172*, 440−451.

Cload, S. T., Richardson, P. L., Huang, Y.-H., & Schepartz, A. (1993) *J. Am. Chem. Soc. 115*, 5005−5014.

Cooney, M., Czernuszewicz, G., Postel, E. H., Flint, S. J., & Hogan, M. E. (1988) *Science 241*, 456−459.

deGennes, P.-G. (1971) *J. Chem. Phys. 5*, 572.

Dewar, M. J. S., & Thiel, W. (1977) *J. Am. Chem. Soc. 99*, 4907.

Doi, M., & Edward, S. F. (1978) *J. Chem. Soc., Faraday Trans. 2*, *74*, 1789.

Drak, J., & Crothers, D. M. (1991) *Proc. Natl. Acad. Sci. U.S.A. 88*, 3074−3078.

Durand, M., Chevrie, K., Chssignol, M., Thuong, N. T., & Maurizot, J. C. (1990) *Nucleic Acids Res. 18*, 6353−6359.

Durland, R. H., Kessler, D. J., Gunnell, S., Duvic, M. D., Pettitt, B. M., & Hogan, M. E. (1991) *Biochemistry*, *30*, 9246−9255.

Fisher, D. E., Parent, L. A., & Sharp, P. A. (1992) *Proc. Natl. Acad. Sci. U.S.A. 89*, 11779−11783.

Goodman, S. D., Nash, H. A. (1989) *Nature 341*, 251−254.

Grigoriev, M., Praseuth, D., Guieysse, A. L., Robin, P., Thuong, N. T., Helene, C., & Harel-Bellan, A. (1993) *Proc. Natl. Acad. Sci. U.S.A. 90*, 3502−3505.

Hagerman, P. J. (1981) *Biopolymers 20*, 1503−1535.

Havre, P. A., Gunther, E. J., Gasparra, E. P., & Glazer, P. M. (1993) *Proc. Natl. Acad. Sci. U.S.A. 90*, 7879−7883.

Hederson, D., & Hurley, L. H. (1995) *Nature Med. 1*, 525−527.

Horikoshi, M., Bertuccioli, C., Takada, R., Wang, J., Yamamoto, T., & Roeder, R. G. (1992) *Proc. Natl. Acad. Sci. U.S.A. 89*, 1060−1064.

Huang, H., Zhu, L., Reid, B. R., Drobny, G. P., & Hopkins, P. B. (1995) *Science 270*, 1842−1845.

Kahn, J. D., & Crothers, D. M. (1992) *Proc. Natl. Acad. Sci. U.S.A. 89*, 6343−6347.

Kahn, J. D., Yun, E., & Crothers, D. M. (1994) *Nature 368*, 163−166.

Kerppola, T. K., & Curran, T. (1991a) *Science 254*, 1210−1214.

Kerppola, T. K., & Curran, T. (1991b) *Cell 66*, 317−324.

Kessler, D. J., Pettitt, B. M., Cheng, Y.-K., Smith, S. R., Jarayaman, K., Vu, H. M., & Hogan, M. E. (1993) *Nucleic Acids Res.* 21, 4810−4815.

Kim, J., Klooster, S., & Shapiro, D. J. (1995) *J. Biol. Chem. 270*, 1282−1288.

Kim, J. L., Nikolov, D. B., & Burley, S. K. (1993) *Nature 365*, 520−527.

Kim, Y., Geiger, J. H., Hahn, S., & Sigler, P. B. (1993) *Nature 365*, 512−520.

Koo, H.-S., Wu, H.-M., & Crothers, D. M. (1986) *Nature 320*, 501−506.

Koo, H.-S., Drak, J., Rice, J. A., & Crothers, D. M. (1990) *Biochemistry 29*, 4227−4234.

Kostrewa, D., Granzin, J., Koch, C., Choe, H. W., Ragkunathan, S., & Wolf, W. (1991) *Nature 349*, 178−180.

Kovacic, R. T., & van Holde, K. E. (1977) *Biochemistry 16*, 1440−1498.

Lerman, L. S., & Frisch, H. L. (1982) *Biopolymers 21*, 995−997.

Levene, S. D., & Crothers, D. M. (1986a) *J. Mol. Biol. 189*, 61−72.

Levene, S. D., & Crothers, D. M. (1986b) *J. Mol. Biol. 189*, 73−83.

Levene, S. D., Wu, H.-M., & Crothers, D. M. (1986) *Biochemistry 25*, 3988−3995.

Levene, S. D., & Zimm, B. H. (1989) *Science 245*, 396−399.

Li, T., Stark, M. R., Johonson, A. D., & Wolberger, C. (1995) *Science 270*, 262−269.

Liberles, D. A., & Dervan, P. B. (1996) *Proc. Natl. Acad. Sci. U.S.A. 93*, 9510−9514.

Lumpkin, O. J., & Zimm, B. H. (1982) *Biopolymers 21*, 2315−2316.

Maher, L. J., III, Wold, B., & Dervan, P. B. (1990) *Biochemistry 29*, 8820−8826.

Martin, J. P., & Espinosa, M. (1993) *Science 260*, 805−807.

Moser, H. E., & Dervan, P. B. (1987) *Science 238*, 645−650.

Muller, H.-P., & Varmus, H. E. (1994) *EMBO J. 13*, 4704−4714.

Olson, W. K., Marky, N. L., Jernigan, R. T., & Zhurkin, V. B. (1993) *J. Mol. Biol. 232*, 530−554.

Rees, W. A., Keller, R. W., Vesenka, J. D., Yang, G., & Bustamante, C. (1993) *Science 260*, 1646−1649.

Schroth, G. P., Cook, G. R., Bradbury, E. M., Gattersfeld, J. M., Schultz, S. C., Shields, G. C., & Steitz, T. A. (1991) *Science 253*, 1001−1007.

Shuey, D. J., & Parker, C. S. (1986) *Nature 323*, 459−461.

Perrouault, L., Asseline, U., Rivalle, C., Thuong, N. T., Bisagni, E., Giovannangeli, C., LeDoan, T., & Helene, C. (1993) *Nature 344*, 358−360.

Pil, P. M., Chow, C. S., & Lippard, S. J. (1993) *Proc. Natl. Acad. Sci. U.S.A. 90*, 9465−9469.

Postel, E. H., Flint, S. J., Kessler, D. J., & Hogan, M. E. (1991) *Proc. Natl. Acad. Sci. U.S.A. 88*, 8227−8231.

Pruss, D., Bushman, F. D., & Wolffe, A. P. (1994) *Proc. Natl. Acad. Sci. USA*, *91*, 5913-5917.

Rice, J. A., Crothers, D. M., Pinto, A. L., & Lippard, S. J. (1988) *Proc. Natl. Acad. Sci. U.S.A. 85*, 4158−4161.

Seela, F., & Kaiser, K. (1987) *Nucleic Acids Res. 15*, 3113−3129.

Shin, C., & Koo, H.-S. (1996) *Biochemistry 35*, 968−972.

Shore, D., & Baldwin, R. L. (1983) *J. Mol. Biol. 170*, 957−981.

Shore, D., Langowski, J., & Baldwin, R. (1981) *Proc. Natl. Acad. Sci. U.S.A. 78*, 4833−4837.

Sun, D., Lin, C. H., & Hurley, L. H. (1993) *Biochemistry 32*, 4487−4495.

Taylor, W. H., & Hagerman, P. J. (1990) *J. Mol. Biol. 212*, 363−376.

Thompson, J. F., & Landy, A. (1988) *Nucleic Acids Res. 16*, 9687−9705.

Wechstler, D. S., & Dang, C. L. (1992) *Proc. Natl. Acad. Sci. U.S.A. 89*, 7635−7639.

Wu, H.-M., & Crothers, D. M. (1984) *Nature 308*, 509−513.

Zhurkin, V. B., Ulyanov, N. B., Gorin, A. A., & Jernigan, R. L. (1991) *Proc. Natl. Acad. Sci. U.S.A. 88*, 7046−7050.

Zinkel, S. S., & Crothers, D. M. (1987) *Nature 328*, 178−181.

BI9624292